Cell Reports

Article

The Foxo1-Inducible Transcriptional Repressor Zfp125 Causes Hepatic Steatosis and Hypercholesterolemia

Graphical Abstract

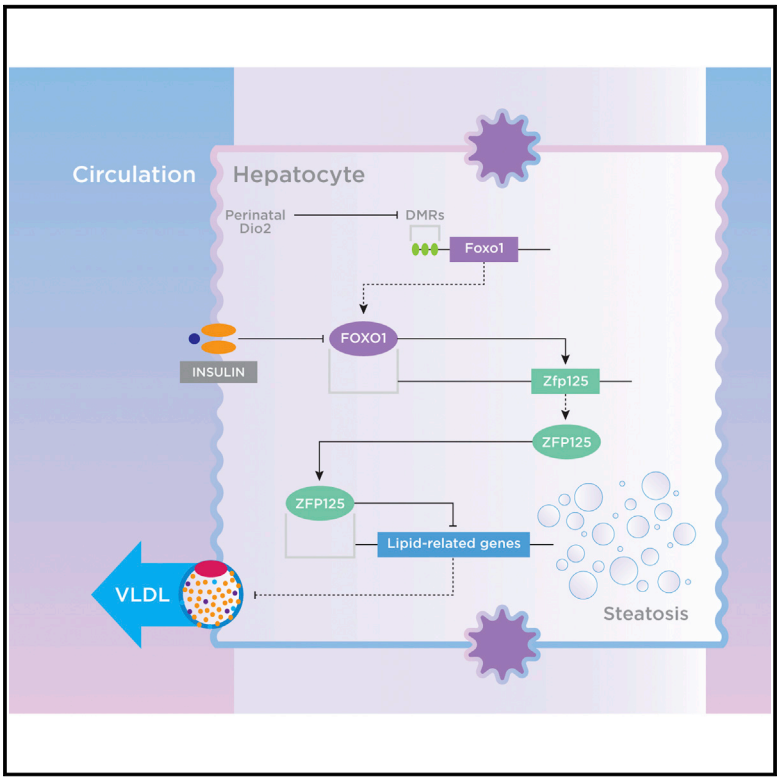

Authors

Gustavo W. Fernandes,
Barbara M.L.C. Bocco,
Tatiana L. Fonseca, ..., Miriam O. Ribeiro,
Balázs Gereben, Antonio C. Bianco

Correspondence

antonio_c_bianco@rush.edu

In Brief

Mice with liver-specific disruption of the type 2 deiodinase gene are resistant to both diet-induced obesity and hepatosteatosis. Fernandes et al. show that this is due to a reduction in liver expression of zinc-finger protein-125, a Foxo1-inducible transcriptional repressor that causes lipid accumulation by reducing hepatic secretion of VLDL.

Highlights

- *Zfp125* is a liver transcriptional repressor of lipid-related genes
- Hepatic *Zfp125* expression is induced by fasting and *Foxo1*
- *Zfp125* reduces lipoprotein assembly and VLDL secretion
- *Zfp125* expression promotes lipid accumulation and liver steatosis in mice

Data and Software Availability

GSE107244

Fernandes et al., 2018, Cell Reports *22*, 523–534
January 9, 2018
https://doi.org/10.1016/j.celrep.2017.12.053

CellPress

Cell Reports
Article

The Foxo1-Inducible Transcriptional Repressor Zfp125 Causes Hepatic Steatosis and Hypercholesterolemia

Gustavo W. Fernandes,[1,2] Barbara M.L.C. Bocco,[1,2] Tatiana L. Fonseca,[1] Elizabeth A. McAninch,[1] Sungro Jo,[1] Lattoya J. Lartey,[1] InSug O-Sullivan,[3] Terry G. Unterman,[3] Nailliw Z. Preite,[4] Robin M. Voigt,[4] Christopher B. Forsyth,[4] Ali Keshavarzian,[4] Richárd Sinkó,[7] Allison B. Goldfine,[5] Mary E. Patti,[5] Miriam O. Ribeiro,[6] Balázs Gereben,[7] and Antonio C. Bianco[1,8,*]
[1]Division of Endocrinology and Metabolism, Rush University Medical Center, Chicago, IL
[2]Program in Translational Medicine, Federal University of Sao Paulo, Sao Paulo, Brazil
[3]Section of Endocrinology, Diabetes and Metabolism, Department of Medicine, University of Illinois at Chicago College of Medicine, Chicago, IL
[4]Division of Digestive Diseases and Nutrition, Rush University Medical Center, Chicago, IL
[5]Joslin Diabetes Center, Harvard Medical School, Boston, MA
[6]Developmental Disorders Program, Center of Biological Science and Health, Mackenzie Presbyterian University, Sao Paulo, Brazil
[7]Department of Endocrine Neurobiology, Institute of Experimental Medicine, Hungarian Academy of Sciences, Budapest, Hungary
[8]Lead Contact
*Correspondence: antonio_c_bianco@rush.edu
https://doi.org/10.1016/j.celrep.2017.12.053

SUMMARY

Liver-specific disruption of the type 2 deiodinase gene (Alb-D2KO) results in resistance to both diet-induced obesity and liver steatosis in mice. Here, we report that this is explained by an ~60% reduction in liver zinc-finger protein-125 (*Zfp125*) expression. *Zfp125* is a *Foxo1*-inducible transcriptional repressor that causes lipid accumulation in the AML12 mouse hepatic cell line and liver steatosis in mice by reducing liver secretion of triglycerides and hepatocyte efflux of cholesterol. *Zfp125* acts by repressing 18 genes involved in lipoprotein structure, lipid binding, and transport. The *ApoE* promoter contains a functional *Zfp125*-binding element that is also present in 17 other lipid-related genes repressed by *Zfp125*. While liver-specific knockdown of *Zfp125* causes an "Alb-D2KO-like" metabolic phenotype, liver-specific normalization of *Zfp125* expression in Alb-D2KO mice rescues the phenotype, restoring normal susceptibility to diet-induced obesity, liver steatosis, and hypercholesterolemia.

INTRODUCTION

The liver metabolizes thyroid hormones via conjugation and deiodination (Visser and Peeters, 2000). The latter is critical given that thyroid hormone is secreted as thyroxine (T4) and must be activated (converted) to T3 via deiodination to gain biological activity. The liver exhibits high levels of the type 1 deiodinase (*D1*), but *D1*-generated T3 equilibrates rapidly with plasma and does not affect local thyroid hormone signaling in hepatocytes (Arrojo E Drigo and Bianco, 2011). In contrast, the other thyroid hormone-activating deiodinase *D2* does increase local thyroid hormone signaling, but it is not expressed in the adult mammalian liver due to *LXR/RXR*-mediated repression (Christoffolete et al., 2010; Kalaany et al., 2005). Interest in this pathway was reawakened recently with the observation that *D2* is expressed transiently in the neonatal mouse liver: hepatic *D2* expression and enzyme activity peaks on post-natal day 1 (P1) and is rapidly silenced by P5 down to background levels. This brief peak of *D2*-generated T3 modifies the methylation pattern and the expression levels of thousands of hepatic genes, increasing future susceptibility to diet-induced obesity and liver steatosis (Fonseca et al., 2015).

A mouse with hepatocyte-specific *D2* inactivation (Alb-D2KO) exhibits lower liver T3 content at birth and a delay in neonatal expression of lipid-related genes. Adult Alb-D2KO animals are less susceptible to liver steatosis, hypertriglyceridemia, and obesity when placed on a high-fat diet (HFD). A microarray study identified 165 genes that are differentially expressed in the adult Alb-D2KO liver, 10%–20% of which contain differential DNA methylation (Fonseca et al., 2015). Among the most differentially expressed genes in the liver of Alb-D2KO mice is the Cys2Hys2 (C2H2) zinc-finger protein 125 (*Zfp125*), previously associated with muscle cell proliferation and transformation (Giorgi et al., 1999).

In the present investigation, we characterized *Zfp125* as a *Foxo1*-inducible hepatic transcriptional repressor that decreases hepatocyte lipid secretion and causes liver steatosis. We also asked whether lower levels of *Zfp125* observed in the adult Alb-D2KO liver could explain the phenotype of resistance to diet-induced obesity and liver steatosis observed in these animals.

RESULTS

Zfp125 Promotes Lipid Accumulation in AML12 Cells

The *Zfp125* gene encodes an ~37-kDa C2H2-type zinc-finger protein (Figure 1A) identified as one of the top-ranking genes

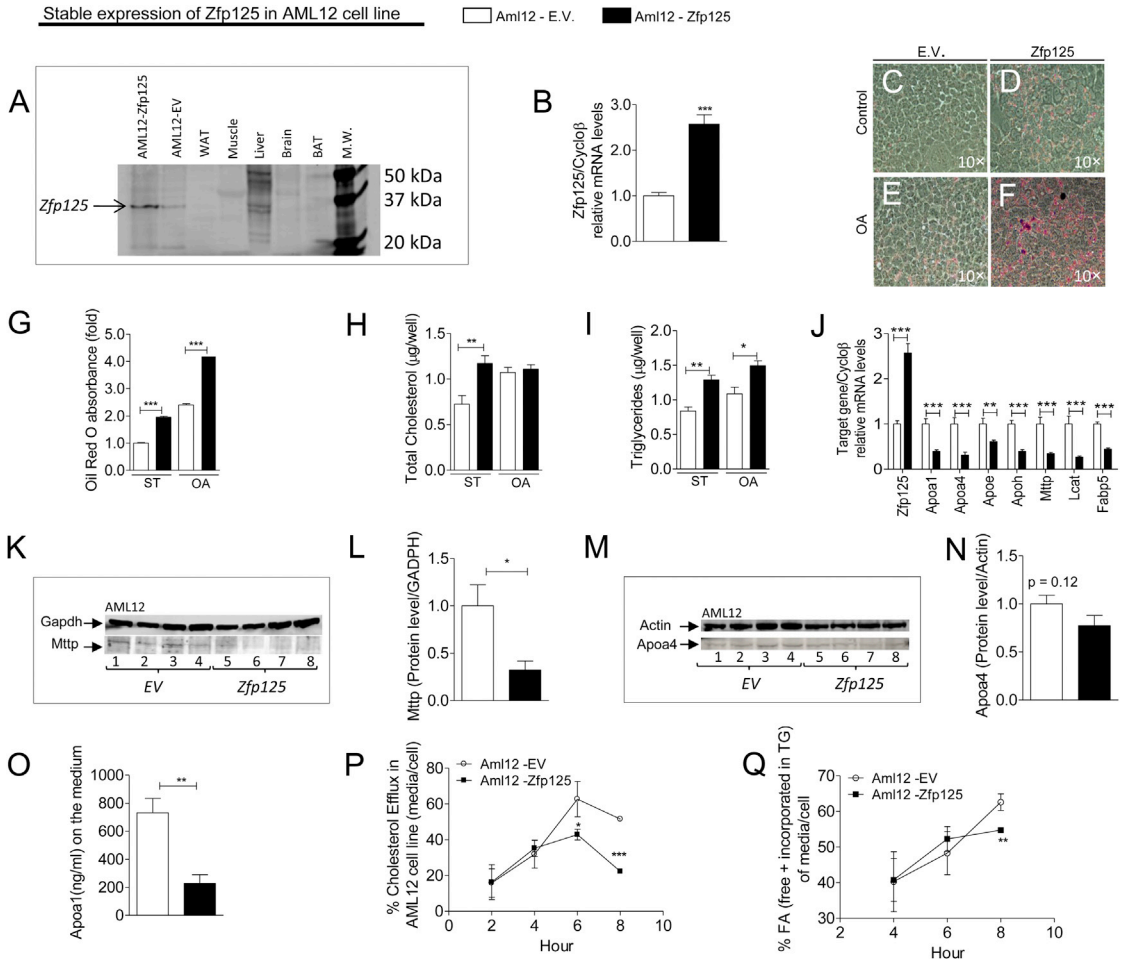

Figure 1. Tissue Distribution and Stable Expression of *Zfp125* in the AML12 Cell Line

(A) Western blot of cells and mouse tissue sonicates probed with α-Zfp125; 30 μg total protein was loaded in each track.

(B) *Zfp125* mRNA levels in cells.

(C–F) Representative cells stained with ORO; in (C) EV and (D) *Zfp125*, cells were treated with control medium; in (E) EV and (F) *Zfp125*, cells were treated with oleic acid (OA).

(G) Absorbance of ORO extracted from cells; ST, standard medium.

(H) Cellular cholesterol content.

(I) Cellular triglycerides content.

(J) mRNA levels assessed by qRT-PCR in cells.

(K) Western blot of cell sonicates probed with α-*Gapdh* and α-*Mttp*; 1, 2, 5, and 6 are from cells kept on standard medium; 3, 4, 7, and 8 are from cells kept on medium containing oleic acid.

(L) Quantification of *Mttp* bands shown in (K), normalized with *Gapdh*.

(M) Western blot of cell sonicates probed with α-*Actin* and α-*Apoa4*; lanes are as in (K).

(N) Quantification of *Apoa4* bands shown in (M), normalized with *Actin*.

(O) *Apoa1* levels in conditioned medium.

(P) Cholesterol efflux in cells.

(Q) Percentage of FA (free plus incorporated in triglyceride) of media/cells. TG, triglycerides.

Values are the mean ± SEM of 3–12 independent samples. Gene abbreviations are in Table S6. *$p < 0.05$, **$p < 0.01$, ***$p < 0.001$ versus respective control.

downregulated in liver of adult Alb-D2KO mice (Fonseca et al., 2015). Western blot studies indicate that liver is the site with highest *Zfp125* expression (Figure 1A). We created the AML12 (alpha mouse liver 12) cell line stably expressing *Zfp125* (AML12-*Zfp125*), which exhibits ~2.5-fold higher expression of *Zfp125* protein levels (Figure 1A) and mRNA (Figure 1B). AML12-*Zfp125* cells visibly accumulate lipids (oil red O [ORO] staining; Figures 1C and 1D), and the neutral lipid content is increased by ~2-fold (Figure 1G) as compared to empty vector (EV)-expressing (AML12-EV) cells. Lipid accumulation results from an ~60% increase in cholesterol (Figure 1H) and ~30% increase in triglyceride content (Figure 1I). Keeping cells in oleic-acid-supplemented medium doubled the overall neutral lipid content and elevated cholesterol content by ~40% without

significantly affecting triglyceride content (Figures 1E–1I). In this setting, expression of *Zfp125* doubled cellular neutral lipid content and elevated triglyceride content by ~25%, while cholesterol content remained unaffected (Figures 1G–1I).

To identify the molecular mediators underlying this phenotype, we analyzed genes differentially expressed in AML12-*Zfp125* cells. 71 genes were differentially expressed (>1.5-fold at $p < 0.001$) in AML12-*Zfp125* versus AML12-EV cells cultured in standard medium (Tables S2 and S3), 50 of which were suppressed and largely related to lipid metabolism (Table S2). Gene set enrichment analysis (GSEA) identified 79 gene sets modified by stable expression of *Zfp125* (false discovery rate [FDR] < 25%, normalized enrichment score [NES] > 1.5; nominal p value <1%; Table S4); 67 gene sets were impoverished and 12 enriched by *Zfp125* expression. Top-ranking gene sets include regulation of lipid metabolism, coagulation, amino acid or steroid metabolism, and gene transcription. That lipid-related genes are targeted by *Zfp125* was confirmed by qRT-PCR, with 40%–80% repression of *Apoa1*, *Apoa4*, *Apoe*, *Apoh*, *Mttp*, *Lcat*, and *Fabp5* (Figure 1J), which are known to play a role in (1) lipid binding and transport and lipoprotein assembly and (2) cellular uptake of cholesterol-containing lipoproteins (Table S1). The impact of these changes in mRNA is illustrated by an ~70% decrease in protein levels of *Mttp* (Figures 1K and 1L) and medium levels of *Apoa1* (Figure 1O); the ~20% decrease in *Apoa4* levels was borderline significant ($p = 0.12$; Figures 1M and 1N). Notably, no changes in lipogenic genes (*Srebf1-2*, *Acaca*, *Thrsp*, *Gpam*, *Agpat2*, *Dgat2*, *Hmgcr*, and *Cyp7a1* mRNA levels) (Figure S1A) or β-oxidation genes (*Acox2*, *Cpt1b*, and *Acadl*) were observed in AML12-*Zfp125* cells (Figure S1A) as assessed by qRT-PCR, except for *Acsl1* identified in the microarray (Table S1). We next tested whether the *Zfp125*-mediated gene repression (Table S1) reduced outgoing lipid transport from the hepatocytes and we found that cholesterol (Figure 1P) hepatocyte efflux rate was much slower in AML12-*Zfp125* cells; fatty acids (FAs; free + incorporated in triglyceride) levels were also downregulated, but to a lesser extent (Figure 1Q).

Of note, opposing phenotypic patterns were observed in AML12 cells in which small interfering RNA (siRNA) reduced *Zfp125* mRNA levels by ~95% (Figure 2A). Visually, cells looked similar (Figures 2B–2E), but neutral lipid content dropped by ~10%–20% (Figure 2F) due to an ~10%–15% decrease in triglyceride levels (Figure 2H); cholesterol levels remained stable (Figure 2G). *Zfp125* knockdown resulted in a 10%–40% increase in mRNA levels for *Apoa1*, *Apoa4*, *Apoe*, and *Fabp5* (Figure 2I), an ~30% increase in *Apoa1* levels in conditioned medium (Figure 2J), and an ~25% increase in cellular levels of *Apoa4* (Figures 2K and 2L).

Zfp125 Is a Transcriptional Repressor

Given that C2H2 zinc-finger proteins commonly function as transcriptional repressors (Margolin et al., 1994; Witzgall et al., 1994), we scanned the promoter of all differentially expressed lipid-related genes in AML12-*Zfp125* cells for the previously identified Zfp-binding consensus sequence 5′-GGGGGT-3′ and found it to be present in 15 such genes, including *Ldlr*, *Scarb1*, *Fabp1/4/5*, *Apoh*, *Apon*, *Apoa1*, *Apoc1/2*, *Saa3*, *Ephx2*, *Azgp1*, *Apof*, and *Mttp* (Table S7). Next, we used chromatin immunoprecipitation (ChIP) to test whether *Zfp*125 binds to a putative response element present ~600 bp upstream of the transcription start site of the *Mttp* promoter (Figure 3A). We found a 1.5-fold enrichment when FLAG-*Zfp125* was pulled down with αFlag (Figure 3B). To verify that *Zfp125* is indeed a transcriptional repressor, we transiently expressed in AML12-*Zfp125* cells a reporter system in which the well-characterized human *ApoE* gene promoter drives a luciferase reporter (pGl3.ME2.Apoe; Figure 3C). As compared with AML12-EV cells, luciferase activity was virtually null when the full *ApoE* promoter fragment containing 3 putative *Zfp125*-binding regions was used (Figure 3C). However, the *Zfp125*-mediated gene repression was only partial when a truncated *ApoE* gene promoter (missing the two upstream putative *Zfp125*-binding regions) was used (Figure 3C).

Hepatic Zfp125 Expression Is Induced by Fasting and via Foxo1

Zfp125 expression in mouse liver exhibits circadian rhythmicity with the acrophase immediately before feeding (Figure 4A). Indeed, fasting doubles *Zfp125* liver expression in mice, with normalization upon re-feeding (Figure 4B). In contrast, exposure of AML12 cells to 20–200 nM insulin for 6 hr resulted in an ~25%–60% reduction in *Zfp125* mRNA levels (Figure 4C) and an ~30%–50% reduction in *Zfp125* protein levels (Figures 4D and 4E). There was no effect of rosiglitazone or clofibrate (Figure S1B), glucagon (Figure S1C), forskolin (Figure S1D), or oleic acid (Figure S1E) on *Zfp125* mRNA levels in AML12 cells.

This pattern of *Zfp125* expression resembles that of *Foxo1*, which is part of the mechanism that allows cells to transition from fed to fasting states. Thus, we next tested whether *Zfp125* expression was regulated via *Foxo1*. In AML12 cells, transient expression of constitutively active *Foxo1* (CA-*Foxo1*) not only elevated *Zfp125* mRNA levels by ~2-fold but also prevented the reduction in *Zfp125* mRNA caused by exposure to 20 nM insulin for 6 hr (Figure 4F). In fact, the *Zfp125* promoter region contains a predicted *Foxo1* responsive element (5′-CTAAACAA-3′) at approximately −2,500 bp 5′ to the transcriptional start site (Figure 4G). In ChIP assays, we detected *Foxo1* binding to this element through a 3.7-fold enrichment in α*Foxo1* pull-downs (Figure 4H). To test whether the *Foxo1* effect is observed *in vivo*, we looked for differences in hepatic *Zfp125* mRNA levels between mice with liver-specific insulin receptor knockout (LIRKO) and mice carrying a combined liver-specific inactivation of *IR* and *Foxo1* (LIRFKO) (Figure 4I). Indeed, *Zfp*125 mRNA levels are ~75% higher in the LIRKO liver (highest *Foxo1* signaling) than in the LIRFKO liver, in which *Foxo1* signaling was inactivated (Figure 4I). These data indicate that *Zfp125* is regulated by an insulin-*Foxo1*-mediated mechanism.

To find out the physiological relevance of the insulin-*Foxo1*-*Zfp125* pathway, we asked whether there is overlap between the *Zfp125* and *Foxo1* effects in the liver. This was addressed by comparing the set of genes differentially expressed in AML12-*Zfp125* cells (microarray Table S8; $p < 0.05$) with the set of genes regulated by *Foxo1* in fasted animals (differentially expressed genes between LIRKO and LIRFKO liver) (Table S9) (O-Sullivan et al., 2015). The analysis indicated that 335 genes are differentially expressed in both conditions (Table S10)

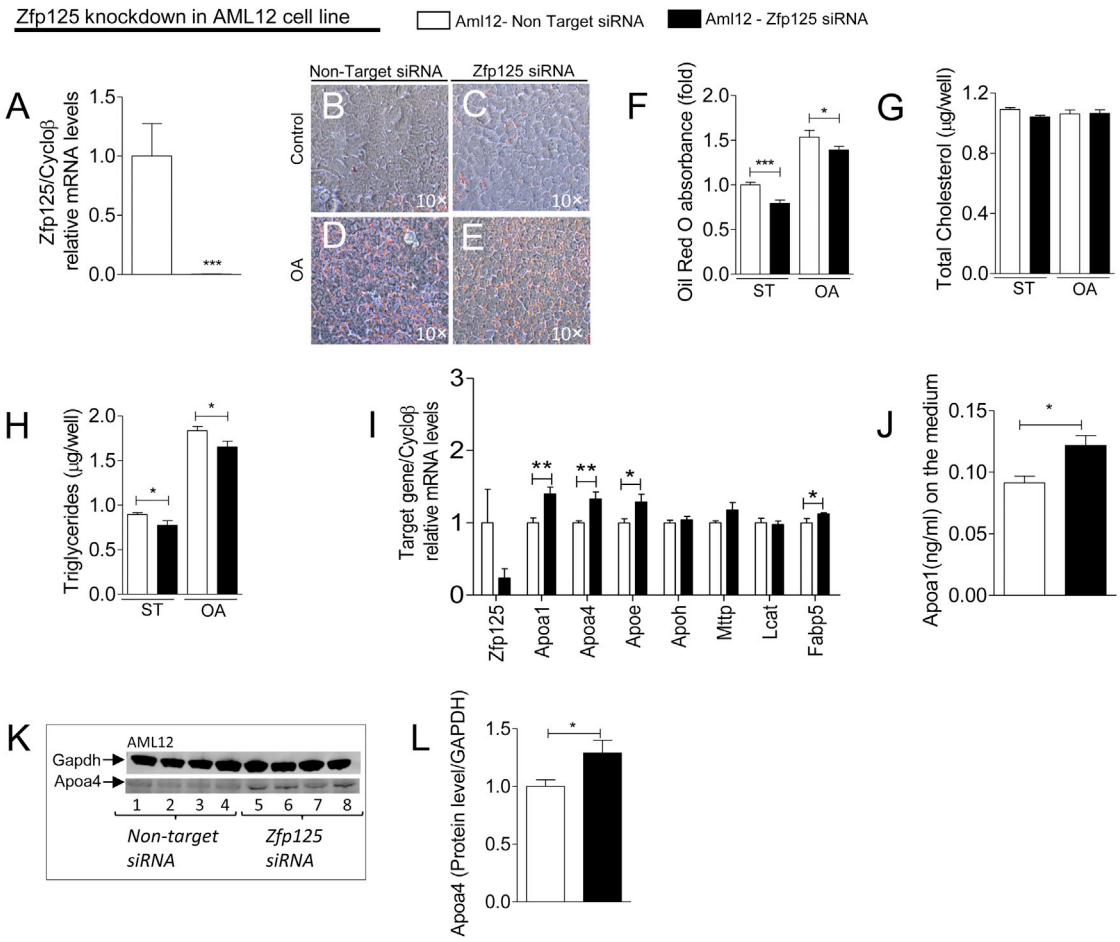

Figure 2. Impact of *Zfp125* Knockdown in the AML12 Cell Line

(A) *Zfp125* mRNA levels in cells.

(B–E) Representative cells stained with ORO; in (B) non-target siRNA and (C) *Zfp125* siRNA, cells were treated with control medium; in (D) non-target siRNA and (E) *Zfp125* siRNA, cells were treated with oleic acid (OA).

(F) Absorbance of ORO extracted from cells; ST, standard medium.

(G) Total cholesterol content.

(H) Total triglyceride content.

(I) mRNA levels assessed by qRT-PCR.

(J) *Apoa1* levels in conditioned medium.

(K) Western blot of cell sonicates probed with α-*Gapdh* and α–*Apoa4*; 1, 2, 5, and 6 are from cells kept on ST, whereas 3, 4, 7, and 8 are from cells kept on OA medium.

(L) Quantification of *Apoa4* bands shown in (K), normalized with *Gapdh*.

Values are the mean ± SEM of 3–12 independent samples. Gene abbreviations are provided in Table S6.*$p < 0.05$, **$p < 0.01$, and ***$p < 0.001$ versus respective control.

(i.e., activation of *Foxo1* or *Zfp125* signaling), of which 91 genes were downregulated by *Zfp125* and by *Foxo1* (Table S10). When processed through the molecular signature database (MSigDB), these genes were implicated in 100 gene pathways (FDR q-value < 0.05; Table S11), including 37 metabolic, 15 catabolic, 13 biosynthetic, and 8 redox pathways. At the same time, 98 genes were downregulated by *Zfp125* and upregulated by *Foxo1* (Table S10), which are involved in 83 MSigDB pathways (FDR q-value < 0.05; Table S11), including 48 cellular housekeeping, 12 metabolic, 12 stress, 6 biosynthetic, and 4 catabolic processes.

Transient Zfp125 Expression in Liver Promotes Hepatosteatosis and Hypercholesterolemia

To assess the role played by Zfp125 *in vivo*, we used liposome-mediated liver-specific delivery of a Zfp125-expressing vector to induce a brief (36 hr) but intense (~8.5-fold) hepatic expression of Zfp125 (Figure 5A). In agreement with the AML-12 cell data, liver sections obtained post-transfection exhibited clusters of perivenular cells containing multiple small fat droplets; these fatty cells were embedded in areas containing cells that were free of fat droplets (Figures 5D and 5E). Such clusters were not observed in liver sections of control animals (Figures 5B and

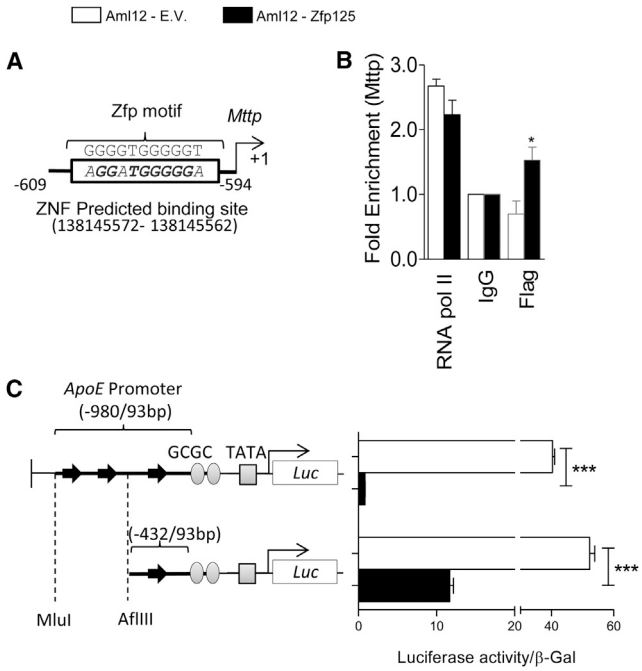

Figure 3. *Zfp125* Is a Transcriptional Repressor

(A) Putative *Zfp125* binding site on the *Mttp* promoter.

(B) Chromatin immunoprecipitation of AML12 cells with α-FLAG antibody followed by qRT-PCR; results are fold enrichment of input with IgG antibody.

(C) AML12 cells were transfected with mouse *Apoe* promotor-reporter constructs carrying a fragment of the mouse *Apoe* promoter lacking the downstream intron (−980/+93 bp) or truncated variant thereof (−432/+93 bp). Luciferase activity was normalized for β-galactosidase activity; thick arrows indicate the *Zfp125* predicted binding sites.

Values are the mean ± SEM of 3–12 independent samples. Gene abbreviations are provided in Table S6. *p < 0.05, **p < 0.01, and ***p < 0.001 versus respective control.

5C). ORO image analysis of these clusters confirmed an ~3.4-fold increase in lipid accumulation when compared with liver sections of animals that received EV (Figure 5F). In this setting, Zfp125 expression reduced the expression of liver Apoa4, Apoc1 and Lcat, Apoe, Apoh, Mttp, Ldlr, Scarb1, Fabp1,4,5, and Azgp1 mRNA levels by ~20%–50% (Figure 5G), plasma Apoa1 levels by ~10% (Figure 5H), Apoa4 levels in the liver by ~35% (Figures 5I and 5J) and Ldlr levels in the liver by ~30% (Figure 5, K-L). Biochemistry analysis of Zfp125-expressing liver revealed a ~50% increase in triglycerides content ($p = 0.09$, Figure 5M) whereas cholesterol content was only minimally affected (Figure 5N), probably due to the limited duration of the experiment. A striking observation in the circulation of mice transiently expressing Zfp125 was an ~35% increase in total cholesterol and an ~2.8-fold increase in VLDL+LDL cholesterol (Figures 5P and 5Q); plasma triglycerides and high-density lipoprotein (HDL) cholesterol levels were not affected (Figures 5O and 5R). To test whether Zfp125 affects liver secretion of triglycerides *in vivo*, we injected Triton (WR1339) in mice transiently expressing Zfp125 in the liver to inhibit lipoprotein lipase and clearance of VLDL. In this scenario, Zfp125 reduced triglyceride secretion rate by ~30% (Figure 5S).

The observation that the Alb-D2KO liver exhibits a 50%–60% reduction in Zfp125 mRNA levels (Figure 6A) and an ~40% reduction in Foxo1 mRNA levels (Figure 4J) led us to hypothesize that liver Zfp125 plays a role in the Alb-D2KO metabolic phenotype. Because the most dramatic Alb-D2KO phenotype is resistance to diet-induced obesity and to liver-steatosis, these studies were performed in animals kept on an HFD. This was tested using a two prong-approach; i.e., transient Zfp125 knockdown or overexpression in mice.

Development of an Alb-D2KO-like Phenotype after Liver-Specific Zfp125 Knockdown

We first placed control mice on HFD for 10 days and subsequently split them into two groups: (1) mice receiving liposome-mediated liver-specific delivery of a Zfp125 siRNA and (2) mice receiving scrambled siRNA. All animals remained on HFD for an additional 5 days while receiving daily injections of the liposome mixtures, which resulted in an ~35% reduction in liver Zfp125 mRNA levels (Figure 6B). Remarkably, by the end of the 15th day, animals transiently expressing Zfp125 siRNA behaved similarly to Alb-D2KO mice kept on the same HFD regimen; i.e., gained much less body weight (Figure 6C), exhibited less liver steatosis (Figures 6D–6I), and accumulated less triglyceride and cholesterol in the liver (Figures 6J and 6K) but did not exhibit the slightly lower plasma triglycerides (Figure 6L) and very low-density lipoprotein (VLDL)/low-density lipoprotein (LDL) (Figure 6N) levels observed in the Alb-D2KO animals kept on HFD.

Liver Zfp125 Expression Rescues the Alb-D2KO Phenotype

We next used an approach similar to that described above by placing Alb-D2KO animals on HFD for 10 days and subsequently splitting them into two groups: (1) mice receiving liposome-mediated liver-specific delivery of a Zfp125-expressing vector and (2) mice receiving an EV. All animals remained on HFD for an additional 5 days while receiving daily injections of the liposome mixtures, which resulted in an ~3-fold elevation in liver Zfp125 mRNA levels compared with control animals (Figure 7A). By the end of the 15th day, Alb-D2KO animals transiently expressing Zfp125 behaved similarly to control mice kept on the same HFD regimen; i.e., gained similar amounts of body weight (Figure 7B), exhibited liver steatosis (Figures 7C–7H) with larger deposits of triglycerides and cholesterol (Figures 7I and 7J), and exhibited higher plasma cholesterol (Figure 7L) and VLDL/LDL (Figure 7M) levels when compared with control animals kept on HFD.

ZNF670 Is the Zfp125 Human Homolog

Using the basic local alignment search tool (BLAST; NCBI), the Zfp125 nucleotide sequence (Figure S2A) was compared against the human reference RNA sequence database. ZNF670 was identified as gene containing the C2H2 domain with the highest score (Figure S2A), the lowest E-value, and an identity of 74% (Table S5). In addition to the C2H2 domain, ZNF670 gene encodes within its N terminus a Kruppel-associated box A domain (KRAB-A box), known in some settings for recruiting co-repressors and other transcription factors (Figure S2A).

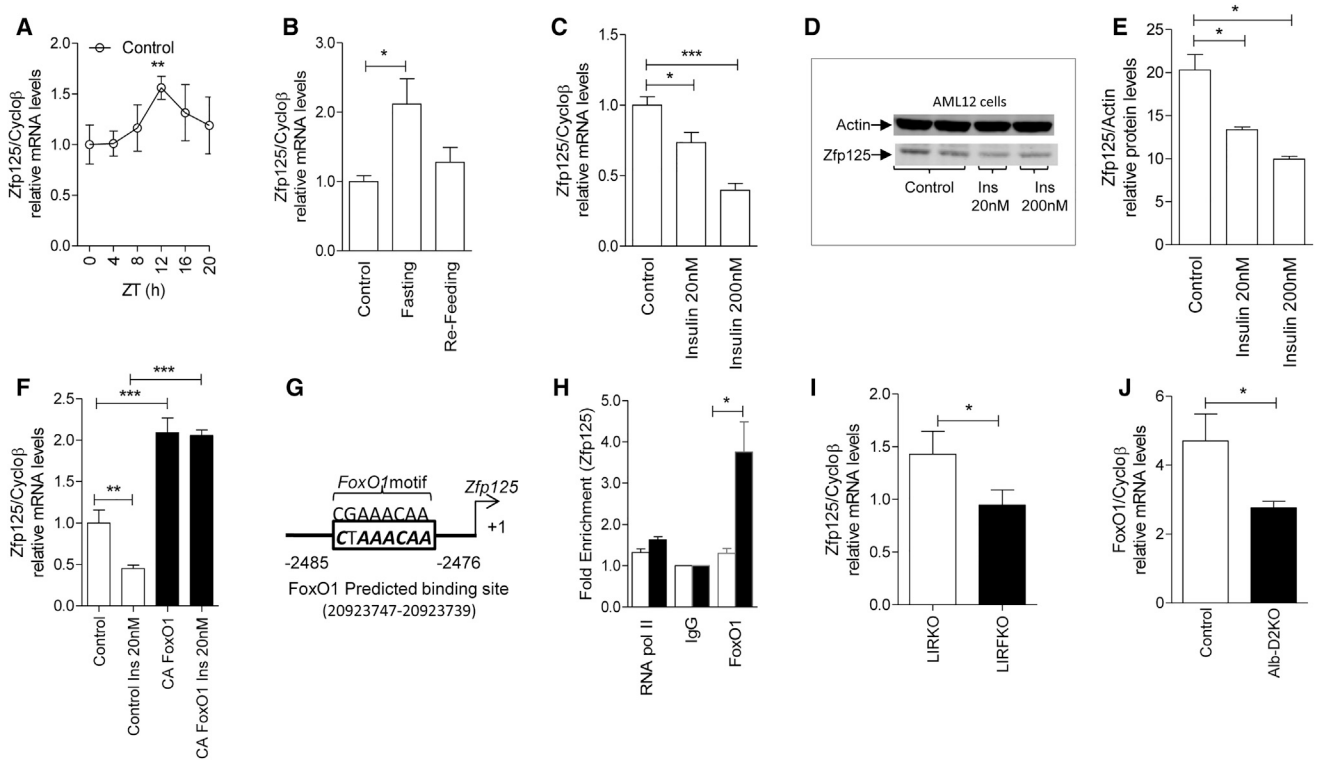

Figure 4. *Zfp125* Expression in Liver and AML12 Cell Line

(A) *Zfp125* mRNA in liver of control mice throughout a 24-hr period; ZT, Zeitgeber.

(B) *Zfp125* mRNA in liver of control, 36-hr fasted, or refed mice.

(C) *Zfp125* mRNA levels in cells treated with 20 nM or 200n M insulin for 6 hr.

(D) Western blot of cell sonicates probed with α-*Actin* and α–*Zfp125*.

(E) Quantification of *Zfp125* bands shown in (D), normalized with *Actin*.

(F) *Zfp125* mRNA levels in cells infected with CA *Foxo1* and control ± 20 nM insulin for 6 hr.

(G) Putative *Foxo1* binding site on *Zfp125* promoter.

(H) Chromatin immunoprecipitation of AML12 cells with α-*Foxo1* antibody followed by qRT-PCR; results are fold enrichment of input with IgG antibody.

(I) *Zfp125* mRNA levels in liver of LIRKO and LIRFKO mice.

(J) *Foxo1* mRNA levels in liver of Alb-D2KO and control mice. For insulin experiments cells were serum starved with 0.1% FBS overnight followed by insulin. Gene abbreviations are provided in Table S6.

Values are the mean ± SEM of 3–10 independent samples. *$p < 0.05$, **$p < 0.01$, and ***$p < 0.001$ versus controls; *$p < 0.05$ and **$p < 0.01$ versus all groups.

A number of experiments in AML12 cells and mice were performed with ZNF670, and the results were very similar to those obtained when Zfp125 was used; namely, ZNF670 causes lipid accumulation in AML12 cells (Figures S2C–S2F) and liver steatosis in mice (Figures S3B–S3E) that is associated with negative regulation of key lipid-related genes (Figures S2J and S3M).

DISCUSSION

The Alb-D2KO mouse is resistant to diet-induced obesity and liver steatosis (Fonseca et al., 2015). Here, we identified the *Foxo1*-inducible gene *Zfp125* as key mediator of this phenotype. *Zfp125* is a liver transcriptional repressor (Figures 3A–3C) that lowers the expression of 18 genes that encode (1) lipoprotein structural or associated components, (2) lipid-binding/transport proteins across cellular membranes, and/or (3) cellular proteins involved in lipoprotein uptake (Table S1). *Zfp125* expression leads to (1) reduction in outgoing hepatocyte/liver lipid transport (Figures 1P and 5S), (2) accumulation of triglycerides and cholesterol in hepatocytes that *in vivo* leads to hepatic steatosis (Figures 5B–5E and 7C–7H), and (3) accumulation of circulating VLDL plus LDL cholesterol levels that results in hypercholesterolemia (Figures 5P, 5Q, 7L, and 7M). There is significant overlap between *Foxo1*- and *Zfp125*-target genes and pathways (Table S10), suggesting that *Zfp125* modulates *Foxo1* actions in liver. These findings provide a plausible mechanism for how a brief perinatal hepatic peak of *D2* modulates susceptibility to obesity, liver steatosis, and hypercholesterolemia later in life.

Zfp125 displays typical characteristics of a transcriptional repressor. It binds to a hexameric element (5′-GGGGGT-3′) (Wagner et al., 2000; Porsch-Ozcurumez et al., 2001) that can be found in the *Mttp* promoter (Figure 3, A-B) and other genes (*Ldlr*, *Scarb1*, *Fabp1/4/5*, *Apoh*, *Apon*, *Apoa1*, *Apoc1/2*, *Saa3*, *Ephx2*, *Azgp1*, *Apof*, and *Mttp* [Table S7] and *Apoe*, *Apoa4*, and *Lcat* [Wagner et al., 2000]) while repressing transcriptional activity of the *ApoE* promoter (Figure 3C). In fact, microarrays

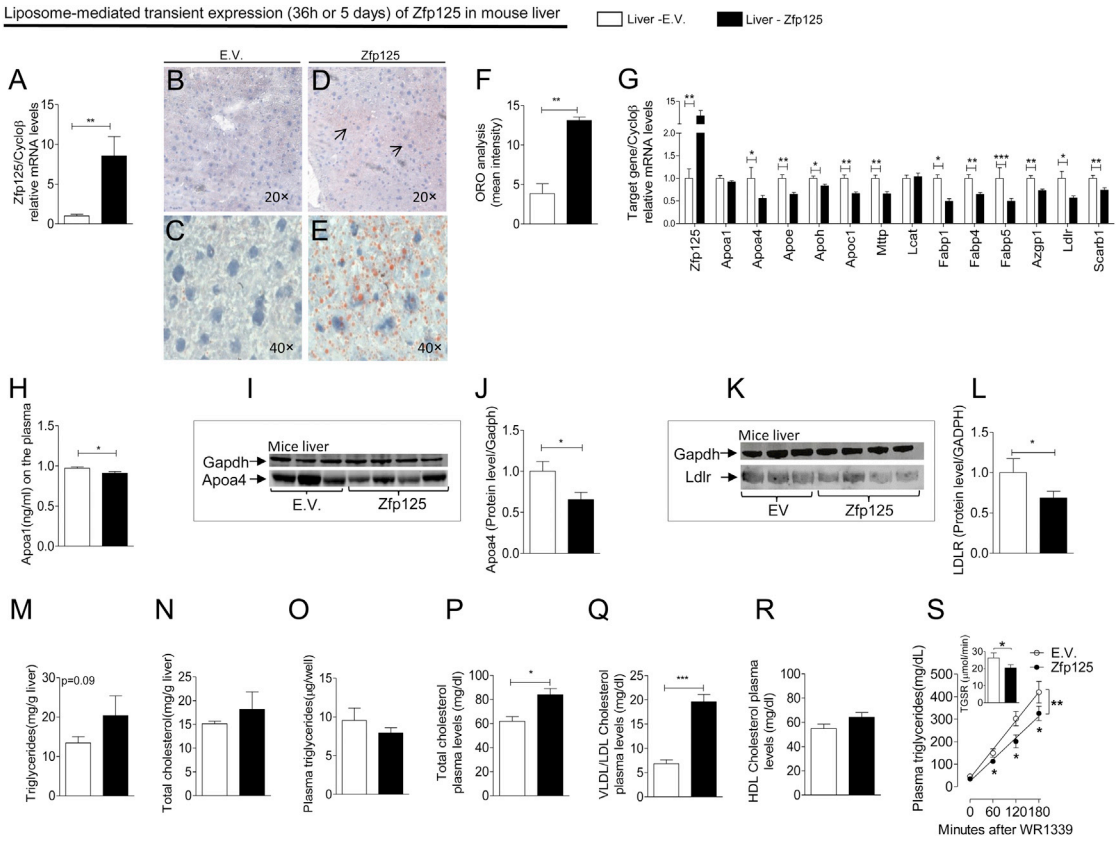

Figure 5. Impact of Transient Expression of *Zfp125* in Mouse Liver

(A) *Zfp125* mRNA levels in liver.

(B–E) Representative liver section stained with ORO. Lipid droplets are indicated by arrows.

(B and D) EV (B) and *Zfp125* (D) with 20x magnification.

(C and E) EV (C) and *Zfp125* (E) with 40x magnification.

(F) Quantification of ORO staining in liver sections; values are mean intensity/image area.

(G) mRNA levels of liver genes assessed by qRT-PCR.

(H) *Apoa1* levels in plasma as measured by ELISA.

(I) Western blot of mice liver probed with α-*Gapdh* and α-*Apoa4*.

(J) Quantification of *Apoa4* bands shown in (I), normalized with *Gapdh*.

(K) Western blot of mice liver probed with α-*Gapdh* and α-*Ldlr*.

(L) Quantification of *Ldlr* bands shown in (K), normalized with *Gapdh*.

(M) Liver triglyceride content.

(N) Liver cholesterol content.

(O) Plasma triglyceride levels.

(P) Total cholesterol plasma levels.

(Q) Plasma levels of VLDL plus LDL cholesterol.

(R) Plasma levels of HDL cholesterol.

(S) Plasma triglycerides in mice transiently expressing *Zfp125* vector (5 days) or EV (5 days) after injection of TritonWR1339. Linear regression lines ($r = 0.995$ and $\alpha = 2.1 \pm 0.10$ for EV; $r = 0.988$ and $\alpha = 1.6 \pm 0.13$ for *Zfp125*) with slopes significantly different ($p = 0.033$). TGSR, triglyceride secretion rate.

Values are mean ± SEM of 3–10 independent samples. Gene abbreviations are provided in Table S6.*$p < 0.05$, **$p < 0.01$, and ***$p < 0.001$ versus respective control.

studies revealed that most gene sets were impoverished and only a few were enriched in hepatocytes stably expressing *Zfp125* (Table S4). *Zfp125*-mediated gene repression correlates well with hepatocyte/liver accumulation of lipids (Figures 1B–1J, 2A–2I, and 5A–5G). Even a relatively brief *in vivo* elevation in *Zfp125* mRNA (36 hr) repressed key lipid transport genes and produced clusters of lipid accumulation in the liver (Figures 5B–5G). Such lipid depots are made up of triglycerides and cholesterol (Figures 1C–1I) and unlikely reflect accelerated synthesis or slower catabolism of these lipids (Figure S1A). Rather, the nature of the genes affected by *Zfp125* (Tables S1 and S2) suggests that slowing outgoing lipid transport is the mechanism. This was confirmed by directly measuring a slower outgoing efflux of cholesterol in AML12 cells stably expressing *Zfp125* (Figure 1P) and slower triglyceride secretion rates in mice transiently expressing *Zfp125* (Figure 5S). Less clear is why VLDL

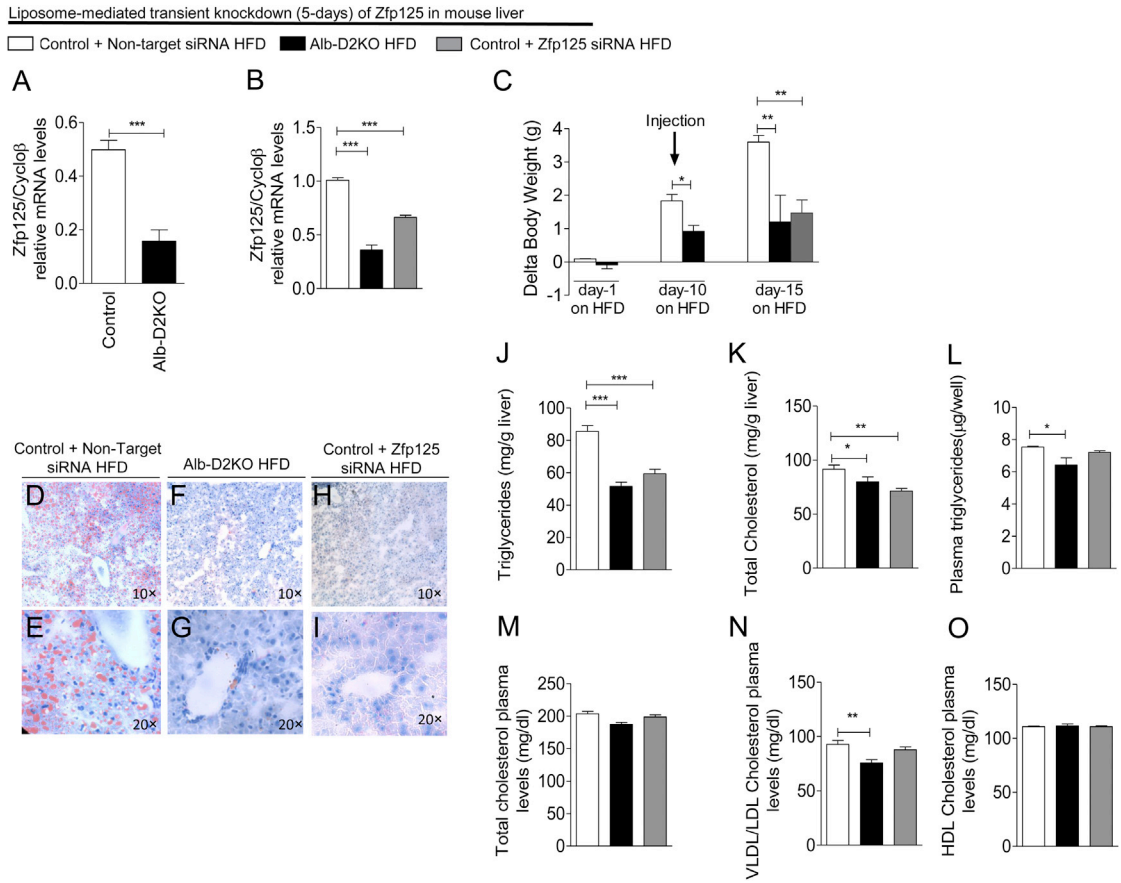

Figure 6. Impact of Transient Knockdown of *Zfp125* in Mouse Liver

(A) *Zfp125* mRNA levels in liver of Alb-D2KO or control mice.

(B) *Zfp125* mRNA levels in control liver transfected with non-target siRNA, Alb-D2KO liver or control liver transfected with *Zfp125* siRNA; animals received daily injections of liposomes for 5 days.

(C) Delta body weight of animals undergoing *Zfp125* mRNA manipulation as indicated during 15 days of HFD; intraperitoneal injection of liposomes started at day 10 as indicated.

(D–I) Representative liver sections stained with ORO. (D) Control+Non-target siRNA HFD, (F) Alb-D2KO HFD, and (H) control+ *Zfp125* siRNA HFD with 10x magnification. (E) Control+Non-target siRNA HFD, (G) Alb-D2KO HFD, and (I) Control+ *Zfp125* siRNA HFD with 20x magnification.

(J) Liver triglyceride content.

(K) Liver cholesterol content.

(L) Plasma triglyceride levels.

(M) Total cholesterol plasma levels.

(N) Plasma levels of VLDL plus LDL cholesterol.

(O) Plasma levels of HDL cholesterol.

Values are mean ± SEM of 4–16 independent samples. Gene abbreviations are provided in Table S6.*$p < 0.05$, **$p < 0.01$, and ***$p < 0.001$ versus respective control.

plus LDL cholesterol is elevated in mice transiently expressing *Zfp125* (Figures 5Q and 7M), but the reduction in hepatic *Ldlr* could play a role (Figures 5K–5L).

Although this was not addressed in the present study, the fact that *Zfp125* expression is downstream of *Foxo1* opens the possibility that *Zfp125* modifies (synergistically or antagonistically) the main actions of *Foxo1* in the liver; i.e., activation of gluconeogenesis, glycogenolysis, VLDL assembly, and secretion (Cheng and White, 2010; Cheng and White, 2011; Kamagate et al., 2008; Matsumoto et al., 2006). Indeed, a comparison between genes affected by *Zfp125* expression and by *Foxo1* (Table S10) identified multiple metabolic and cellular pathways, but not on cell cycle or apoptosis (Tables S11 and S12). However, it is striking that *Zfp125* and *Foxo1* have opposite effects on *Mttp* expression (Figure 1, J and L) and triglyceride secretion (Figure 1Q). In addition, even though both *Foxo1* (Matsumoto et al., 2006) and *Zfp125* cause liver steatosis in mice, they do it through different mechanisms. While *Foxo1* acts by stimulating fatty acid synthesis and slowing down fatty acid oxidation (Matsumoto et al., 2006; Cheng and White, 2011), *Zfp125* decreases triglyceride and cholesterol secretion (Figures 1P and 5S). The contrast in these effects is reminiscent of the dual role *Foxo1*

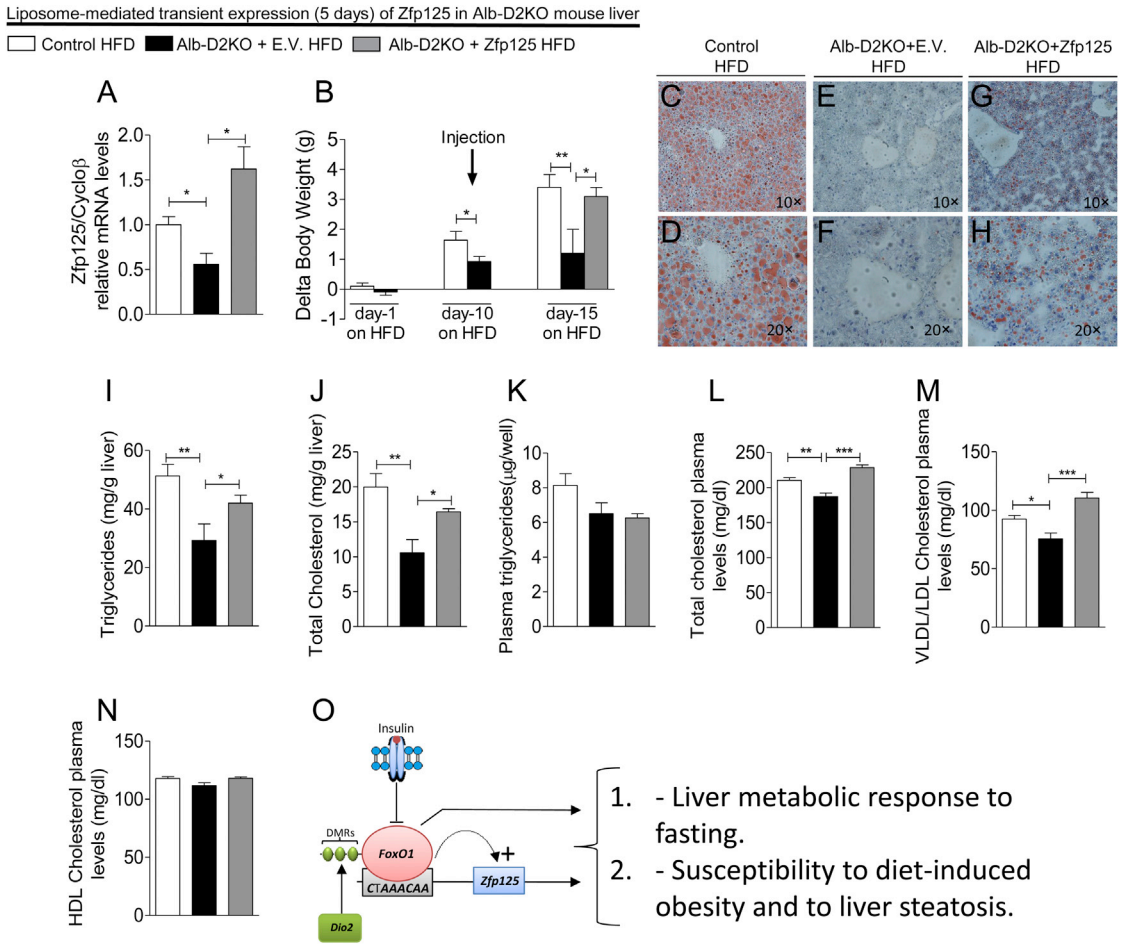

Figure 7. Impact of Transient Expression of *Zfp125* in Alb-D2KO Mouse Liver

(A) *Zfp125* mRNA levels in control, Alb-D2KO expressing EV, or Alb-D2KO expressing *Zfp125* vector; animals received daily injections of liposomes for 5 days.

(B) Delta body weight of animals undergoing *Zfp125* mRNA manipulation as indicated during 15 days of HFD; intraperitoneal injection of liposomes started at day 10 as indicated.

(C–H) Representative liver sections stained with ORO. (C) Control HFD, (E) Alb-D2KO+EV HFD, and (G) Alb-D2KO+ *Zfp125* HFD with 10x magnification. (D) Control HFD, (F) Alb-D2KO+EV HFD. and (H) Alb-D2KO+ *Zfp125* HFD with 20x magnification.

(I) Liver triglycerides content.

(J) Liver cholesterol content.

(K) Plasma triglyceride levels.

(L) Total cholesterol plasma levels.

(M) Plasma levels of VLDL plus LDL cholesterol.

(N) Plasma levels of HDL cholesterol.

(O) Proposed mechanism by which neonatal Dio2 expression affects methylation status (DMR) of the Foxo1 gene and consequently *Zfp125* expression, explaining the metabolic phenotype of Alb-D2KO mice.

Values are mean ± SEM of 4–9 independent samples. Gene abbreviations are provided in Table S6. *$p < 0.05$, **$p < 0.01$, and ***$p < 0.001$ versus respective control.

plays in controlling hepatic insulin sensitivity and lipid metabolism (Matsumoto et al., 2006).

Elimination of the perinatal surge in hepatocyte *D2* affects, later in life, liver expression of ~165 genes involved in lipid metabolism (Fonseca et al., 2015). Between 10% and 20% of these genes exhibit differentially methylated regions (DMRs) and thus qualify as epigenetic modifications caused by *Dio2* inactivation. One such gene is *Foxo1*, where we identified 3 positive DMRs associated with active chromatin (Fonseca et al., 2015) (Figure 7O); *Foxo1* mRNA levels are reduced by ~40% in adult Alb-D2KO liver (Figure 4J). Given the sensitivity of *Zfp125* expression to *Foxo1*, it is not surprising that *Zfp125* mRNA levels are reduced in the Alb-D2KO liver (Figure 6A). Thus, the critical question is how much of the Alb-D2KO metabolic phenotype can be attributed to decreased expression of *Zfp125*. First, we looked at gene sets enriched in the Alb-D2KO liver microarrays and found "lipoprotein binding," "lipid homeostasis," and "lipid transport" among the top gene sets (Fonseca et al., 2015); these

sets contain genes repressed by *Zfp125* (Table S1). Second, we showed that liver-specific *Zfp125* knockdown in control mice leads to an Alb-D2KO-like phenotype of resistance to diet-induced obesity and to liver steatosis (Figures 6B–6K). Third, we showed that liver-specific *Zfp125* expression in Alb-D2KO mice rescues their metabolic phenotype (Figures 7A–7N), restoring normal sensitivity to diet-induced obesity and liver steatosis (Fonseca et al., 2015).

A previously identified zinc-finger protein *ZNF202* functions as a transcriptional repressor of *Apoc1/c2/e* and *Apoa1/c3/a4* when overexpressed in mouse hepatoma cells *mhAT3F2* (Vrins et al., 2013) and of *Abca1* and *Abcg1* when transfected in HepG2 cells (Porsch-Ozcurumez et al., 2001). In mice, transient hepatic expression of *ZNF202* increases serum HDL-cholesterol levels (Vrins et al., 2013). Furthermore, a polymorphism in *ZNF259* was associated with sex-specific changes in serum lipid levels, such as LDL cholesterol (Aung et al., 2014). Contrary to *Zfp125*, *Zfp202* mRNA levels (the mouse homolog of *ZNF202*) are not modified in the Alb-D2KO liver (Figure S1F) and is not stimulated by fasting (Figure S1G), and its effects are predominantly on cholesterol metabolism (Schmitz et al., 2004; Vrins et al., 2013). In contrast, the set of genes repressed by *Zfp125* (Table S1) underlies a phenotype of lipid accumulation and liver steatosis, as well as hypercholesterolemia. Taken together, these findings suggest that a group of physiologically relevant hepatic zinc-finger proteins exists that regulates different aspects of fatty acid and cholesterol homeostasis by suppressing the expression of key genes involved in these pathways.

To understand the underlying mechanisms that explain the Alb-D2KO metabolic phenotype, we identified the *Foxo1*-inducible *Zfp125* pathway in the liver. *Zfp125* reduces hepatocyte and liver lipid secretion and promotes liver steatosis. Furthermore, *Zfp125* affects the expression of hundreds of *Foxo1*-regulated genes, potentially modifying the hepatocyte transition from fed to fasting states (Figure 7O).

EXPERIMENTAL PROCEDURES

All experiments were planned according to the American Thyroid Association guide to investigating thyroid hormone economy and action in rodent and cell models (Bianco et al., 2014) and were approved by the Institutional Animal Care and Use Committee at Rush University Medical Center as described previously (Fonseca et al., 2015).

DNA Constructs and Cell Experiments

AML-12 mouse hepatocytes (American Type Culture Collection) were cultured with DMEM/F-12 medium (GIBCO) supplemented with 5 μg/ml insulin, 5 μg/mL transferrin, 5 ng/mL selenium (ITS; GIBCO), and 40 ng/mL dexamethasone (DEX) (all from Sigma). In order to create subclones that stably express *Zfp125*, *ZNF670* or EV (BG188, pCI-Neo; Promega), expression vectors were created. The *Zfp125* expression construct (BG631) was generated by gene synthesis (Blue Heron) based on the *Zfp125* coding sequence (GenBank: AJ005350). The fragment was cloned between NheI and EcoRI of the pCI-Neo vector (Promega), and a 5′ FLAG epitope was added. The *ZNF670* expression construct (BG660) was created by cloning the human *ZNF670* (GenBank: NM_033213) cDNA with Phusion polymerase PCR (Thermo Fisher Scientific) on a template of HepG2 cells and inserted between NheI and EcoRI of the pCI-Neo vector, and an 5′ FLAG epitope was added. For the gene reporter assay, pGL3Basic-ME.2/ApoEpromoter was acquired as a gift from Sohail Tavazoie (plasmid 51436; Addgene). Its truncated version (BG729) was generated by cutting the plasmid with MluI and AflII, removing 1,145 bp from the original pGL3Basic-ME.2/ApoEpromoter, blunting, and reattaching. Constructs were confirmed by sequencing. BG631, BG660, or BG188 were transfected into AML12 cells using Lipofectamine 2000 (Thermo Fisher Scientific) following selection with G418 (500 μg/mL) for 7 days. The functionality of each specific plasmid was confirmed by qRT-PCR. For *Zfp125* knockdown, a pool siRNA oligonucleotides were designed and synthesized by Dharmacon (GE Healthcare). The sequences of these siRNA oligonucleotides are listed in Table S6. *Zfp125* siRNA and non-target siRNA were transfected into cells using DharmaFECT1 transfection reagent (GE Dharmacon). Adenoviral particles expressing WT- and CA-*Foxo1* expressing constructs (Lartey et al., 2015) were transiently expressed in cells. Cells were plated at 2.5×10^5 cells/well in 6-well dishes and transduced with adenoviral particles at 2.0 × 1,010 pfu/mL and 1.8 × 1010 pfu/mL, respectively, diluted in 1 mL serum-free DMEM. Complete medium containing 10% fetal bovine serum (FBS) was added after 6 hr and changed again after 24 hr. After 43 hr, medium was replaced with fresh medium containing 0.1% FBS (no ITS).

In some experiments (as indicated), cells were treated with 0.1 mM oleic acid-BSA solution (Sigma) during 48 hr; medium was changed every 24 hr. Control cells were maintained in oleic-acid-free medium. In other experiments, cells cultured for 24 hr with 0.1% FBS (no ITS) were treated with 20 or 200 nM insulin (Sigma) or 20 nM glucagon (Sigma) during 6 hr; other treatments included 300 μM clofibrate (Sigma) or 1 μM rosiglitazone (Sigma) dissolved in DMSO during 5 hr. Control cells were treated with vehicle.

ORO Cell Staining

As indicated, cells were stained with ORO (Sanchez-Hidalgo et al., 2007) and examined under a light microscope (Nikon Eclipse TS100). ORO was quantified through colorimetry after extraction with 1 mL 100% isopropanol for 10 min, followed by gentle vibration to release ORO from cells (Lin et al., 2007). The extract from individual wells was then transferred to a 96-well plate and absorbance measured at 500 nm using Bio-Rad iMark Microplate. The quantification of ORO intensity in representative liver sections was done using NIS Element software. ORO intensity was measured by selecting the color threshold of the ORO droplet and results expressed as mean intensity/area.

Lipid Efflux Assay

Cholesterol efflux was measured using a Cholesterol Efflux Assay Kit (Cell-based) (Abcam). Briefly, cells were plated in a 96-well white plate with 100 μL media/well and 8 hr later washed with FBS-free media. Labeling reagent and equilibration buffer were mixed and added to cells that were incubated overnight at 37°C with media containing 0.1% FBS. The next morning, cells were washed with FBS-free media and then kept in media containing 10% FBS at 37°C. At the indicated times (i.e., 2, 4, 6, and 8 hr), supernatant was transferred to a new 96-well white plate and fluorescence measured (excitation wavelength [Ex]/emission wavelength [EM] = 482/515 nm). The cell monolayer was solubilized with cell lysis buffer and fluorescence measured (Ex/EM = 482/515 nm). Efflux (%) was calculated by dividing fluorescence intensity of media by fluorescence intensity of cells (× 100). An FA (free + incorporated in triglyceride) assay was measured similarly, using an FA uptake assay (Abcam, ab176768). Cells were plated in 96-well black plates with 100 μL media/well and incubated overnight in 0.1% FBS media. Cells were treated with 0.1 mM oleic acid for 2, 4, 6, and 8 hr. Supernatants were transferred to a new 96-well black plate and cell monolayers solubilized with cell lysis buffer. Fatty acid labeling solution was added to cells and supernatant fractions, incubated for 30min and fluorescence measured (Ex/EM = 485/515 nm). Efflux (%) was calculated and expressed as above.

Microarray Analysis

RNA obtained from cells stably expressing *Zfp125* was extracted with the RNeasy Mini Kit (QIAGEN) and processed for microarray at the Joslin Diabetes Center Genomics Core Laboratory (Boston, MA). Gene expression was evaluated using Mouse Gene 2.0 ST arrays (Affymetrix, Santa Clara, CA). Gene expression data were preprocessed using Affymetrix Expression Console. Differential expression analysis was performed in Affymetrix Transcriptome Analysis Console (TAC) to identify individual genes and gene ontology analysis was used to determine differences in enrichment of gene sets between phenotypes (GSEA, Broad Institute). The analysis was performed considering an FDR <25%, an NES >1.5, and a nominal p value < 1%. To compare differentially expressed genes from the microarray analysis of AML12-*Zfp125*

versus AML12-EV against the microarray analysis of LIRFKO mice versus LIRKO mice, individual genes (p value < 5%) were entered into VENNY (http://bioinfogp.cnb.csic.es/tools/venny/index.html). Gene sets were subsequently analyzed utilizing MSigDB (http://software.broadinstitute.org/gsea/msigdb/annotate.jsp) and the overlap computed using the collection C5 (gene sets that contain genes annotated by the same Gene Ontology term), with an FDR q-value < 0.05.

ChIP Assay

ChIP assays were performed using an EZ-Chip Kit (Millipore). Chromatin lysates were prepared, precleared with Protein-A/G agarose beads, and immunoprecipitated with antibodies against FLAG (Sigma), RNA polymerase II (Millipore), or normal mouse immunoglobulin G (IgG) (Millipore) as previously described (Lartey et al., 2015). Beads were extensively washed before reverse crosslinking. DNA was purified and subsequently analyzed by qRT-PCR using primers flanking the proximal binding sites located in the mouse *Mttp and Zfp125* promoters.

Luciferase Gene Reporter Assay

AML12-*Zfp125* cells or AML12-EV were transfected with pGL3Basic-ME.2/*ApoE* promoter or its truncated version missing the two upstream putative Zfp125-binding sites (BG729). 24 hr later, cells were processed for luciferase activity using the Dual-Luciferase Reporter (DLRTM) Assay System (Promega).

Animal Experiments

Unless indicated otherwise, all animals were 8-week-old male C57BL/6J mice that were kept at room temperature (22°C), with a 12-hr dark/light cycle. Alb-D2KO mice (C57BL/6J background) and littermate controls were obtained and maintained as described previously (Fonseca et al., 2015). Liver samples of male LIRKO and LIRFKO mice on a mixed (C57BL/6-FVB/N) background were obtained as described previously (O-Sullivan et al., 2015). Animals were euthanized by asphyxiation in a CO_2 chamber. For the study of circadian rhythmicity, mice were killed on different Zeitgeber time (ZT; 0, 4, 8, 12, 16, and 20 hr), the liver was removed, and RNA was extracted for gene expression analysis; time of the onset of light is referred to as ZT0, while the time of lights off is referred to as ZT12. 36-hr-fasting experiments were performed as described previously (Lartey et al., 2015).

Liposome-Mediated Liver Transfection

In vivo transfections were performed with a liver transfection kit (Altogen Biosystems) and a liposome lipid-based formulation optimized for *in vivo* administration with targeted liver delivery; plasmids and siRNA were transfected into male C57BL/6J or Alb-D2KO mice according to the manufacturer's protocol via intraperitoneal injection. As indicated, C57BL/6J mice that had been kept on chow diet were injected with *Zfp125* expressing vector or EV at 0 and 12 hr and killed at the 36-hr time point. In another set of experiments, C56BL/6J mice that had been kept on chow diet were transfected with *ZNF670* expressing vector or EV at 0, 24, 48, 72, and 96 hr and killed at the 120-hr time point. For the AlbD2KO phenotype recovery experiment, control and Alb-D2KO mice were kept on HFD for a total of 15 days. Starting from the 10th day, Alb-D2KO mice were transiently transfected with *Zfp125* expressing vector or EV daily, while animals were kept on HFD. All Alb-D2KO mice received a total of 5 liposome mix injections on the 10th, 11th, 12th, 13th, and 14th days of the experiment; animals were killed on the 15th day. To generate an AlbD2KO-like phenotype, similarly treated C56BL/6J mice were transfected with *Zfp125* siRNA or non-target siRNA. All liposome-mediated liver transfection experiments were performed with mice kept with food *ad libitum* and fed.

Hepatic Triglyceride Secretion

Mice were fasted during 6 hr. Triton WR 1339 (Sigma) in 10% saline solution was administered via intraperitoneal injection at 500 mg/kg, as indicated previously (Forrest et al., 2013; Hirano et al., 2001). Blood samples were drawn hourly over a 3-hr period in heparin capillary tubes immediately prior to injection and at 1, 2, and 3 hr following injection. Plasma was prepared and processed for triglyceride measurement.

Analytical Studies

Biochemical Analyses and Histology

Blood was collected into EDTA tubes and plasma was separated by centrifugation. Plasma triglycerides were measured by enzymatic colorimetric assay (Abcam, ab65336). Plasma cholesterol fraction was assessed using the Cholesterol Assay Kit (Abcam, ab65390). Briefly, separation of HDL and LDL plus VLDL cholesterol was performed by mixing 100 μL plasma with 100 μL 2× precipitation buffer followed by a 10-min incubation at room temperature and centrifugation for 10 min at 2,000 × *g*. The supernatants (HDL fraction) were transferred to a new tube and pellets resuspended in PBS (VLDL plus LDL fraction). Cholesterol colorimetric assays were performed in all fractions. Plasma and medium *Apoa1* levels were quantified by *Apoa1* Mouse ELISA Kit (Antibodies-online). Cellular and liver triglycerides and cholesterol contents were measured using enzymatic colorimetric assay (Abcam, ab65336 and ab65390). Immediately after killing, liver samples were embedded in optimum cutting temperature (OCT), frozen with dry ice, and stored at −80°C to perform ORO staining.

Gene Expression Analysis

RNA was obtained as described previously (Fonseca et al., 2015). Specific mRNA levels were quantified by qRT-PCR (StepOnePlus real time PCR system, Applied Bioscience) using SYBR Green Supermix (Quanta Biosciences). Standard curves consisting of 4–5 points of serially diluted mixed experimental and control group cDNA were included, and the coefficient of correlation was consistently >0.98, with an amplification efficiency of 80%–110%. The primers are listed in Table S6, with *Cyclob* as internal control (Figure S2).

Western Blot Analysis

Cell/tissue sonicates were obtained as described previously (Lartey et al., 2015). The lysates were diluted with 4× sample loading buffer (Invitrogen) and 5–25 μg total protein was run on 4%–12% NuPAGE BisTris gels (Life Technologies). Samples were transferred to Immobilon-FL PVDF transfer membrane (Millipore) and probed with antibodies as indicated at a 1:1,000 dilution overnight. Fluorescent-labeled secondary antibodies (LI-COR Biosciences) were used at 1:2,500 for 1 hr. All blots were imaged using the LI-COR Odyssey instrument per the manufacturer's instructions.

Zfp125 Antibody

α-Zfp125 was generated by ImmunoGenes Kft (Budakeszi, Hungary). In short, transgenic rabbits (Tg) with enhanced neonatal Fc receptor (FcRn) activity (Baranyi et al., 2013) were immunized as described previously (Dudok et al., 2015) using a keyhole limpet hemocyanin (KLH)-conjugated with the ∼80% conserved polypeptide N′-C-SNGPYKGPVYEKPFDFPS-C′ in Zfp125 and ZNF670; the first C is an extra amino acid required for KLH coupling.

Statistics

All data points are mean ± SEM and were prepared using PRISM (GraphPad Software, San Diego, CA). One-way ANOVA was used to compare more than two groups, followed by the Student-Newman-Keuls' test to detect differences between groups. The Student's t test was used when only two groups were part of the experiment; $p < 0.05$ was used to reject the null hypothesis.

DATA AND SOFTWARE AVAILABILITY

The accession number for all microarray data performed on AML12-*Zfp125* is GEO: GSE107244.

SUPPLEMENTAL INFORMATION

Supplemental Information includes three figures and 11 tables and can be found with this article online at https://doi.org/10.1016/j.celrep.2017.12.053.

ACKNOWLEDGMENTS

We thank Cezar Bianchi and Sarah J. Peterson for their valuable input, comments, and advice. This work was supported by the NIDDK (grant DK65055 to A.C.B., grant R01DK106193 to M.E.P., and grant P30DK 036836 to the Diabetes Research Center, Joslin), the EU (H2020 "Thyrage" 666869), the Hungarian Brain Research Program (grant KTIA_13_NAP_A_I/4 to B.G.), Fundacao de Amparo a Pesquisa do Estado de Sao Paulo (FAPESP)

(grant 2011/21847-6 to M.O.R.), and Coordenadoria de Apoio a Pesquisa (CAPES), Brazil.

AUTHOR CONTRIBUTIONS

G.W.F. designed research, conducted experiments, analyzed data, and prepared the manuscript. B.M.L., C.B, T.L.F., E.A.M., and S.J. conducted experiments and analyzed data. L.J.L. performed the ChIP assay; I.O., N.Z.P., R.M.V., C.B.F., and R.S. conducted experiments; T.G.U., A.K., A.B.G., and M.E.P. conducted experiments and analyzed data. M.O.R. reviewed the manuscript. B.G. created expression vectors for *Zfp125* and *ZNF670*, provided input about *Zfp125*, and reviewed the manuscript. A.C.B. directed all experiments and prepared the manuscript.

DECLARATION OF INTERESTS

The authors declare no competing interests.

Received: April 20, 2017
Revised: November 15, 2017
Accepted: December 15, 2017
Published: January 9, 2018

REFERENCES

Arrojo E Drigo, R., and Bianco, A.C. (2011). Type 2 deiodinase at the crossroads of thyroid hormone action. Int. J. Biochem. Cell Biol. *43*, 1432–1441.

Aung, L.H., Yin, R.X., Wu, D.F., Wang, W., Wu, J.Z., and Liu, C.W. (2014). Sex-specific association of the zinc finger protein 259 rs2075290 polymorphism and serum lipid levels. Int. J. Med. Sci. *11*, 471–478.

Baranyi, M., Cervenak, J., Bender, B., and Kacskovics, I. (2013). Transgenic rabbits that overexpress the neonatal Fc receptor (FcRn) generate higher quantities and improved qualities of anti-thymocyte globulin (ATG). PLoS ONE *8*, e76839.

Bianco, A.C., Anderson, G., Forrest, D., Galton, V.A., Gereben, B., Kim, B.W., Kopp, P.A., Liao, X.H., Obregon, M.J., Peeters, R.P., et al.; American Thyroid Association Task Force on Approaches and Strategies to Investigate Thyroid Hormone Economy and Action (2014). American Thyroid Association Guide to investigating thyroid hormone economy and action in rodent and cell models. Thyroid *24*, 88–168.

Cheng, Z., and White, M.F. (2010). Foxo1 in hepatic lipid metabolism. Cell Cycle *9*, 219–220.

Cheng, Z., and White, M.F. (2011). Targeting Forkhead box O1 from the concept to metabolic diseases: lessons from mouse models. Antioxid. Redox Signal. *14*, 649–661.

Christoffolete, M.A., Doleschall, M., Egri, P., Liposits, Z., Zavacki, A.M., Bianco, A.C., and Gereben, B. (2010). Regulation of thyroid hormone activation via the liver X-receptor/retinoid X-receptor pathway. J. Endocrinol. *205*, 179–186.

Dudok, B., Barna, L., Ledri, M., Szabó, S.I., Szabadits, E., Pintér, B., Woodhams, S.G., Henstridge, C.M., Balla, G.Y., Nyilas, R., et al. (2015). Cell-specific STORM super-resolution imaging reveals nanoscale organization of cannabinoid signaling. Nat. Neurosci. *18*, 75–86.

Fonseca, T.L., Fernandes, G.W., McAninch, E.A., Bocco, B.M., Abdalla, S.M., Ribeiro, M.O., Mohácsik, P., Fekete, C., Li, D., Xing, X., et al. (2015). Perinatal deiodinase 2 expression in hepatocytes defines epigenetic susceptibility to liver steatosis and obesity. Proc. Natl. Acad. Sci. USA *112*, 14018–14023.

Forrest, L.M., Lough, C.M., Chung, S., Boudyguina, E.Y., Gebre, A.K., Smith, T.L., Colvin, P.L., and Parks, J.S. (2013). Echium oil reduces plasma triglycerides by increasing intravascular lipolysis in apoB100-only low density lipoprotein (LDL) receptor knockout mice. Nutrients *5*, 2629–2645.

Giorgi, S., Polimeni, M., Senni, M.I., De Gregorio, L., Dragani, T.A., Molinaro, M., and Bouché, M. (1999). Isolation and characterization of the murine zinc finger coding gene, ZT2: expression in normal and transformed myogenic cells. Gene *230*, 81–90.

Hirano, T., Takahashi, T., Saito, S., Tajima, H., Ebara, T., and Adachi, M. (2001). Apoprotein C-III deficiency markedly stimulates triglyceride secretion in vivo: comparison with apoprotein E. Am. J. Physiol. Endocrinol. Metab. *281*, E665–E669.

Kalaany, N.Y., Gauthier, K.C., Zavacki, A.M., Mammen, P.P., Kitazume, T., Peterson, J.A., Horton, J.D., Garry, D.J., Bianco, A.C., and Mangelsdorf, D.J. (2005). LXRs regulate the balance between fat storage and oxidation. Cell Metab. *1*, 231–244.

Kamagate, A., Qu, S., Perdomo, G., Su, D., Kim, D.H., Slusher, S., Meseck, M., and Dong, H.H. (2008). FoxO1 mediates insulin-dependent regulation of hepatic VLDL production in mice. J. Clin. Invest. *118*, 2347–2364.

Lartey, L.J., Werneck-de-Castro, J.P., O-Sullivan, I., Unterman, T.G., and Bianco, A.C. (2015). Coupling between nutrient availability and thyroid hormone activation. J. Biol. Chem. *290*, 30551–30561.

Lin, C.L., Huang, H.C., and Lin, J.K. (2007). Theaflavins attenuate hepatic lipid accumulation through activating AMPK in human HepG2 cells. J. Lipid Res. *48*, 2334–2343.

Margolin, J.F., Friedman, J.R., Meyer, W.K., Vissing, H., Thiesen, H.J., and Rauscher, F.J., 3rd. (1994). Krüppel-associated boxes are potent transcriptional repression domains. Proc. Natl. Acad. Sci. USA *91*, 4509–4513.

Matsumoto, M., Han, S., Kitamura, T., and Accili, D. (2006). Dual role of transcription factor FoxO1 in controlling hepatic insulin sensitivity and lipid metabolism. J. Clin. Invest. *116*, 2464–2472.

O-Sullivan, I., Zhang, W., Wasserman, D.H., Liew, C.W., Liu, J., Paik, J., Depinho, R.A., Stolz, D.B., Kahn, C.R., Schwartz, M.W., and Unterman, T.G. (2015). FoxO1 integrates direct and indirect effects of insulin on hepatic glucose production and glucose utilization. Nat. Commun. *6*, 7079.

Porsch-Ozcurumez, M., Langmann, T., Heimerl, S., Borsukova, H., Kaminski, W.E., Drobnik, W., Honer, C., Schumacher, C., and Schmitz, G. (2001). The zinc finger protein 202 (ZNF202) is a transcriptional repressor of ATP binding cassette transporter A1 (ABCA1) and ABCG1 gene expression and a modulator of cellular lipid efflux. J. Biol. Chem. *276*, 12427–12433.

Sanchez-Hidalgo, M., Lu, Z., Tan, D.X., Maldonado, M.D., Reiter, R.J., and Gregerman, R.I. (2007). Melatonin inhibits fatty acid-induced triglyceride accumulation in ROS17/2.8 cells: implications for osteoblast differentiation and osteoporosis. Am. J. Physiol. Regul. Integr. Comp. Physiol. *292*, R2208–R2215.

Schmitz, G., Heimerl, S., and Langmann, T. (2004). Zinc finger protein ZNF202 structure and function in transcriptional control of HDL metabolism. Curr. Opin. Lipidol. *15*, 199–208.

Visser, T.J., and Peeters, R.P. (2000). Metabolism of thyroid hormone. In Endotext, L.J. De Groot, P. Beck-Peccoz, G. Chrousos, K. Dungan, A. Grossman, J.M. Hershman, C. Koch, R. Mclachlan, M. New, and R. Rebar, et al., eds. (MDText.com), pp. 81–103.

Vrins, C.L., Out, R., van Santbrink, P., van der Zee, A., Mahmoudi, T., Groenendijk, M., Havekes, L.M., van Berkel, T.J., Willems van Dijk, K., and Biessen, E.A. (2013). Znf202 affects high density lipoprotein cholesterol levels and promotes hepatosteatosis in hyperlipidemic mice. PLoS ONE *8*, e57492.

Wagner, S., Hess, M.A., Ormonde-Hanson, P., Malandro, J., Hu, H., Chen, M., Kehrer, R., Frodsham, M., Schumacher, C., Beluch, M., et al. (2000). A broad role for the zinc finger protein ZNF202 in human lipid metabolism. J. Biol. Chem. *275*, 15685–15690.

Witzgall, R., O'Leary, E., Leaf, A., Onaldi, D., and Bonventre, J.V. (1994). The Krüppel-associated box-A (KRAB-A) domain of zinc finger proteins mediates transcriptional repression. Proc. Natl. Acad. Sci. USA *91*, 4514–4518.